The preconditioning of major sudden stratospheric warmings

S. Bancalá,[1] K. Krüger,[1] and M. Giorgetta[2]

Received 25 August 2011; revised 22 November 2011; accepted 14 December 2011; published 16 February 2012.

[1] The preconditioning of major sudden stratospheric warmings (SSWs) is investigated with two long time series using reanalysis (ERA-40) and model (MAECHAM5/MPI-OM) data. Applying planetary wave analysis, we distinguish between wavenumber-1 and wavenumber-2 major SSWs based on the wave activity of zonal wavenumbers 1 and 2 during the prewarming phase. For this analysis an objective criterion to identify and classify the preconditioning of major SSWs is developed. Major SSWs are found to occur with a frequency of six and seven events per decade in the reanalysis and in the model, respectively, thus highlighting the ability of MAECHAM5/MPI-OM to simulate the frequency of major SSWs realistically. However, from these events only one quarter are wavenumber-2 major warmings, representing a low (∼0.25) wavenumber-2 to wavenumber-1 major SSW ratio. Composite analyses for both data sets reveal that the two warming types have different dynamics; while wavenumber-1 major warmings are preceded only by an enhanced activity of the zonal wavenumber-1, wavenumber-2 events are either characterized by only the amplification of zonal wavenumber-2 or by both zonal wavenumber-1 and zonal wavenumber-2, albeit at different time intervals. The role of tropospheric blocking events influencing these two categories of major SSWs is evaluated in the next step. Here, the composite analyses of both reanalysis and model data reveal that blocking events in the Euro-Atlantic sector mostly lead to the development of wavenumber-1 major warmings. The blocking–wavenumber-2 major warming connection can only be statistical reliable analyzed with the model time series, demonstrating that blocking events in the Pacific region mostly precede wavenumber-2 major SSWs.

Citation: Bancalá, S., K. Krüger, and M. Giorgetta (2012), The preconditioning of major sudden stratospheric warmings, *J. Geophys. Res.*, *117*, D04101, doi:10.1029/2011JD016769.

1. Introduction

[2] The vertical propagation of planetary waves from the troposphere into the stratosphere and their interaction with the zonal mean flow is recognized to be the essential dynamical mechanism responsible for the development of SSWs [*Matsuno*, 1971]. Only anomalously intense planetary waves are able to propagate into the high-latitude stratosphere, in contrast to steady waves of small or moderate intensity which are refracted toward the low-latitude stratosphere [*Matsuno*, 1970]. These planetary-scale disturbances, which are almost always present in the Northern Hemisphere (NH) winter, are a consequence of the inhomogeneity of the Earth's surface [*Reed*, 1963]. Different types of SSWs exist. *Labitzke* [1977] grouped these midwinter disturbances into three categories: *major*, *minor*, and *Canadian* midwinter warmings. A fourth type of warming, the *final* (major) warming, is then responsible for the reversal from the winter to the summer stratospheric circulation, which is characterized by easterly winds at the polar cap. By the World Meteorological Organization (WMO) definition [*Andrews et al.*, 1987], a major midwinter SSW occurs when the zonal mean zonal wind $\bar{u}$ at 60°N becomes easterly and the temperature gradient between 60°N and 90°N reverses at 10 hPa or below during midwinter. On the basis of this WMO criterion, major and final SSWs are necessarily identified by the wind reversal. While minor warmings are observed in both hemispheres, major SSWs occur mainly in the NH, with only one event observed in the Southern Hemisphere 2002 since regular stratospheric observations began in 1957 [*Krüger et al.*, 2005; *Naujokat and Roscoe*, 2005]. *Labitzke et al.* [2002] investigated in detail the occurrence of major SSWs between the 1957 and 2002 period, summarizing 45 years of monitoring the northern winter stratosphere, including the previous WMO mandate to alert the stratospheric community by daily "Stratalerts" during NH winter. Their goal was to forecast the occurrence of these events on the basis of anomalous amplification of planetary waves (amplitude and fluxes) of zonal wavenumber-1 or -2 in the lower to middle stratosphere (50 to 10 hPa). Analyzing this preconditioning, *Labitzke* [1977, 1981] found that an amplification of the zonal wavenumber-1 component concurrently with a minimum of the wavenumber-2 component is a characteristic precondition before the onset of a major warming.

[1]GEOMAR, Helmholtz Centre for Ocean Research Kiel, Kiel, Germany.
[2]Max Planck Institute for Meteorology, Hamburg, Germany.

0148-0227/12/2011JD016769

However, some events may also develop through the amplification of the zonal wavenumber-2 component, as happened in February 1963, January 1985, and February 1989 [e.g., *Finger and Teweles*, 1964; *Naujokat and Labitzke*, 1993]. On the basis of this different wave behavior, the major SSWs were classified as wavenumber-1 or wavenumber-2 warmings depending on which zonal wavenumber was responsible for the poleward eddy heat transport leading to the warming [*Naujokat et al.*, 2002; *Krüger et al.*, 2005]. The enhanced planetary wave activity is the first step of the following wave-mean flow interaction, which precedes the warming of the stratosphere by typically a few weeks [*Newman et al.*, 2001].

[3] In the prewarming phase, tropospheric blocking events, which are large-scale ridges in the jet stream associated with a strong high-pressure system at the surface, involve strong, long-lasting, quasi-stationary distortion of the tropospheric flow and are able to modulate the upward propagation of planetary waves that induce a major SSW [*Labitzke*, 1965; *O'Neill and Taylor*, 1978; *Quiroz*, 1986]. *Naujokat et al.* [2002] found westward propagating Normal mode Rossby wave activity after the onset of Atlantic blocking events, leading to wave-wave interactions, maximum heat flux and the breakup of the polar vortex in December 1987 and December 2001. Depending on the location of the tropospheric blocking events, different planetary waves can play a role. *Martius et al.* [2009] and *Castanheira and Barriopedro* [2010] showed that Euro-Atlantic blocking events generally cause an amplification of the zonal wavenumber-1, while Pacific blocking events are associated with an amplification of the zonal wavenumber-2. In addition, *Garfinkel et al.* [2010] reported that geopotential height anomalies can enhance the wavenumber-1 or the wavenumber-2 Eliassen-Palm flux, weakening the polar vortex nearly immediately.

[4] In this study, we focus our analysis on the preconditioning of major warmings in the NH stratosphere. We develop an objective identification algorithm that permits one to distinguish between wavenumber-1 and wavenumber-2 major SSWs. This aim is in contrast to recent papers which basically concentrated on the breakup phase of the polar vortex, influencing the surface via the stratosphere-troposphere downward coupling mechanism after major SSWs [*Charlton and Polvani*, 2007; *Charlton et al.*, 2007; *Butchart et al.*, 2010, 2011]. Although individual events have been analyzed in detail [*Labitzke*, 1981; *Mukougawa and Hirooka*, 2004; *Krüger et al.*, 2005; *Manney et al.*, 2008, 2009], a statistical analysis of the preconditioning of major SSWs in reanalysis or in model data has, to the best of our knowledge, not yet been carried out. Finally, the possible role of tropospheric blocking events influencing major SSWs in the prewarming phase is examined. This is in contrast to previous tropospheric blocking studies, which either characterized major SSWs based on the postwarming phase [*Martius et al.*, 2009; *Castanheira and Barriopedro*, 2010; *Woollings et al.*, 2010] or did not distinguish between different types of SSW events [*Taguchi*, 2008]. The paper is structured as follows. The data and methodology used are described in section 2. In section 3, the statistical analysis of the preconditioning of major SSWs connected with tropospheric blocking events, using reanalysis and model data, is presented. General conclusions and implications for future work are drawn in section 4.

2. Data and Methodology

2.1. Data

[5] The analyses are based on two long time series using daily data from the European Centre for Medium-Range Weather Forecasts (ECMWF) Re-Analysis (ERA-40) and the coupled atmosphere ocean model MAECHAM5/MPI-OM for the October to May period.

[6] The ERA-40 reanalysis is interpolated onto a 2.5° × 2.5° regular horizontal grid with 60 model levels in the vertical (L60), extending from the surface up to 0.1 hPa, and 6-h time interval. Data are available from 1 September 1957 to 31 August 2002, thus 45 NH winter seasons are analyzed. More detailed information about the ERA-40 assimilation can be found in the work of *Uppala et al.* [2005].

[7] The coupled atmosphere ocean general circulation model MAECHAM5/MPI-OM was developed at the Max Planck Institute (MPI) for Meteorology in Hamburg. MAECHAM5 is the middle atmosphere model configuration of ECHAM5 [*Manzini et al.*, 2006; *Roeckner et al.*, 2006] with a vertical domain extending up to 0.01 hPa (∼80 km), thus including the full stratosphere and the lower part of the mesosphere. The model is used at horizontal resolution T63 corresponding to a Gaussian grid of ∼1.9° × 1.9° and with 47 vertical layers (L47), of which nine are between 110 hPa and 10 hPa and 12 between 10 and 0.01 hPa [*Giorgetta et al.*, 2007]. The model includes gravity wave parameterizations (GWP) and the related momentum fluxes to represent the internal variability of the middle atmosphere. The effects of subgrid-scale orography variations on the atmospheric flow are considered in the GWP developed by *Lott and Miller* [1997] and *Lott* [1999], while the Hines-GWP [*Hines*, 1997a, 1997b] takes into account the simulation of nonorographic gravity waves. More details about the GWP in MAECHAM models are described by *Manzini et al.* [1997]. For the ocean-sea ice model MPI-OM, a standard horizontal grid with grid spacing of 1.5° (GR15) is used for the horizontal domain [*Jungclaus et al.*, 2006], while the vertical resolution has 40 levels (L40) with level thickness increasing with depth. For the setup of the uncoupled ocean model, two data sets are used: the German Ocean Model Intercomparison Project (OMIP) climatology and the NCEP/NCAR atmospheric forcing from the NCEP/NCAR reanalysis. After the uncoupled spinup of the ocean model, atmosphere and ocean are coupled by means of the Ocean-Atmosphere-Sea Ice-Soil (OASIS) coupler. The MAECHAM5/MPI-OM model does not require any flux correction [*Jungclaus et al.*, 2006]. More detailed information regarding the MPI-OM can be found in the work of *Jungclaus et al.* [2006] and *Wetzel et al.* [2010]. The use of a coupled middle atmosphere model, in which the atmosphere-ocean interactions are interactively taken into account, should lead to an improved representation of the stratospheric winter circulation, in particular in the simulation and in the frequency of major SSWs, which are influenced by the land-sea contrast and, e.g., by the El Niño-Southern Oscillation (ENSO) phenomenon [*Manzini et al.*, 2006].

Table 1. Major SSWs Identified in the ERA-40 Data Set[a]

Number	Central Date	Type
1	31 January 1958	W_1
2	15 January 1960	W_1
3	28 January 1963	W_2
4	1 April 1965	W_2
5	16 December 1965	W_1
6	23 February 1966	W_1
7	7 January 1968	W_2
8	28 November 1968	W_1
9	13 March 1969	W_1
10	1 January 1970	W_1
11	18 January 1971	W_2
12	19 March 1971	W_1
13	31 January 1973	W_1
14	9 January 1977	W_1
15	22 February 1979	W_2
16	29 February 1980	W_1
17	4 March 1981	W_1
18	4 December 1981	W_1
19	1 January 1985	W_2
20	23 January 1987	W_1
21	7 December 1987	W_1
22	15 December 1998	W_1
23	26 February 1999	W_1
24	20 March 2000	W_1
25	11 February 2001	W_1
26	30 December 2001	W_1
27	17 February 2002	W_1

[a]Reported is the central date of the major warmings and their classification as obtained with our algorithm. The types W_1 and W_2 indicate major SSWs of wavenumber-1 and wavenumber-2, respectively.

[8] For this study, a 160-year control simulation has been performed. The atmospheric model was initialized with constant pre-industrial greenhouse gas concentrations from 1860 and an ozone climatology for pre-1980 levels [*Fortuin and Kelder*, 1998]. The ocean model was set up with a control experiment of CMIP3 (Coupled Model Intercomparison Project 3). Note that this version of the MAECHAM5/MPI-OM model does not have an internal generated quasi-biennial oscillation nor a solar cycle is included in this control run. Owing to the spinup period of the coupled model, the last 100 years of the simulation are analyzed.

2.2. The Major SSW Criterion

[9] An objective criterion to identify and characterize the preconditioning of major SSWs is developed. The algorithm first identifies the major SSWs then classifies them depending on their planetary wave activity during the prewarming phase.

2.2.1. Identifying Major SSW Events

[10] A major warming is identified by the reversal of $\bar{u}$ at 10 hPa and 60°N, with the first day of easterlies defined as the *central date* of the warming. As after the onset of the warming $\bar{u}$ may fluctuate between weak easterlies and westerlies, to prevent counting the same event twice, *Charlton and Polvani* [2007] introduced a 20 day mask starting from the central date within which no other major SSW is counted. In our algorithm, this 20 day interval, which approximately equals two radiative timescales at 10 hPa (i.e., the time necessary for the restoring of the polar vortex) [*Newman and Rosenfield*, 1997], starts instead from the first day of westerly winds after the central date. Additionally, if the first day after this 20 day mask has easterly wind, the algorithm searches for the next day with westerly wind exceeding 5 m/s and starts from that day to search for other major SSWs. These additional constraints are introduced because occasionally the wind fluctuates around the zero value during the recovery of the vortex, thus it should avoid counting mere wind oscillations as major SSWs. In order to avoid the overestimation of spring major SSWs, we also modified the final warming detection criterion of *Charlton and Polvani* [2007]. To distinguish major SSWs from final warmings the algorithm considers the number of consecutive days of westerlies and the wind intensity after major warming events. Cases after which $\bar{u}$ becomes westerly for at least 10 consecutive days, but during which the wind does not reach, at least for 1 day, the intensity of 5 m/s, are assumed to be final warmings, and as such are discarded.

[11] Different to the WMO definition, which considers only major midwinter SSWs between November and February, our criterion detects major SSWs during the whole stratospheric winter circulation season between October and May. This permits us to address a more persistent stratospheric winter circulation either because of (1) a delay of the polar vortex breakup in spring observed since the 1980s due to ozone and CO_2 changes [e.g., *Langematz et al.*, 2003] or (2) the common cold pole bias problem in middle atmospheric models [*Pawson et al.*, 2000]. Table 1 lists all major SSWs identified with the new algorithm in the ERA-40 data set.

2.2.2. Classifying Major SSW Events

[12] Once a major SSW is identified, the algorithm classifies it as a preconditioned wavenumber-1 (W_1) or wavenumber-2 (W_2) warming. This involves the analysis of planetary waves; therefore zonal Fourier-analyzed geopotential height fields Z_n of wavenumbers n = 1–3 as well as the wave components of the heat fluxes $v'T'_n$ are calculated as described by *Pawson and Kubitz* [1996]. To distinguish the preconditioning of the major SSWs, it is necessary to define a time interval in which the enhanced wave amplitudes Z_n and the relative heat flux components $v'T'_n$ should be detected. Therefore a 10-day window period is considered around day D, that is, within 14 days preceding the central date, the day for which the difference of $\bar{u}$ at 10 hPa and 60°N between that day and 5 days later is strongest. This length of the time interval is chosen because it roughly corresponds to the time for planetary wave to propagate from the troposphere to the stratosphere [see *Limpasuvan et al.*, 2004, Figure 5]. To characterize a major SSW, the algorithm checks for each of the days falling in the time period $D-7$ to $D+3$, which of the following conditions are satisfied.

1) W_1 major SSW:

- $Z_1 > Z_2$ (10 hPa, 60°N)

2) W_2 major SSW:

- $\nabla Z = Z_2 - Z_1 > 100$ m (50 hPa, 60°N)

- $\nabla v'T' = v'T'_2 - v'T'_1 > 15$ K m/s (100 hPa, 60°N)

3) W_3 major SSW:

- $Z_3 > Z_1$ and $Z_3 > Z_2$ (50 hPa, 60°N)

- $v'T'_3 > v'T'_1$ and $v'T'_3 > v'T'_2$ (100 hPa, 60°N)

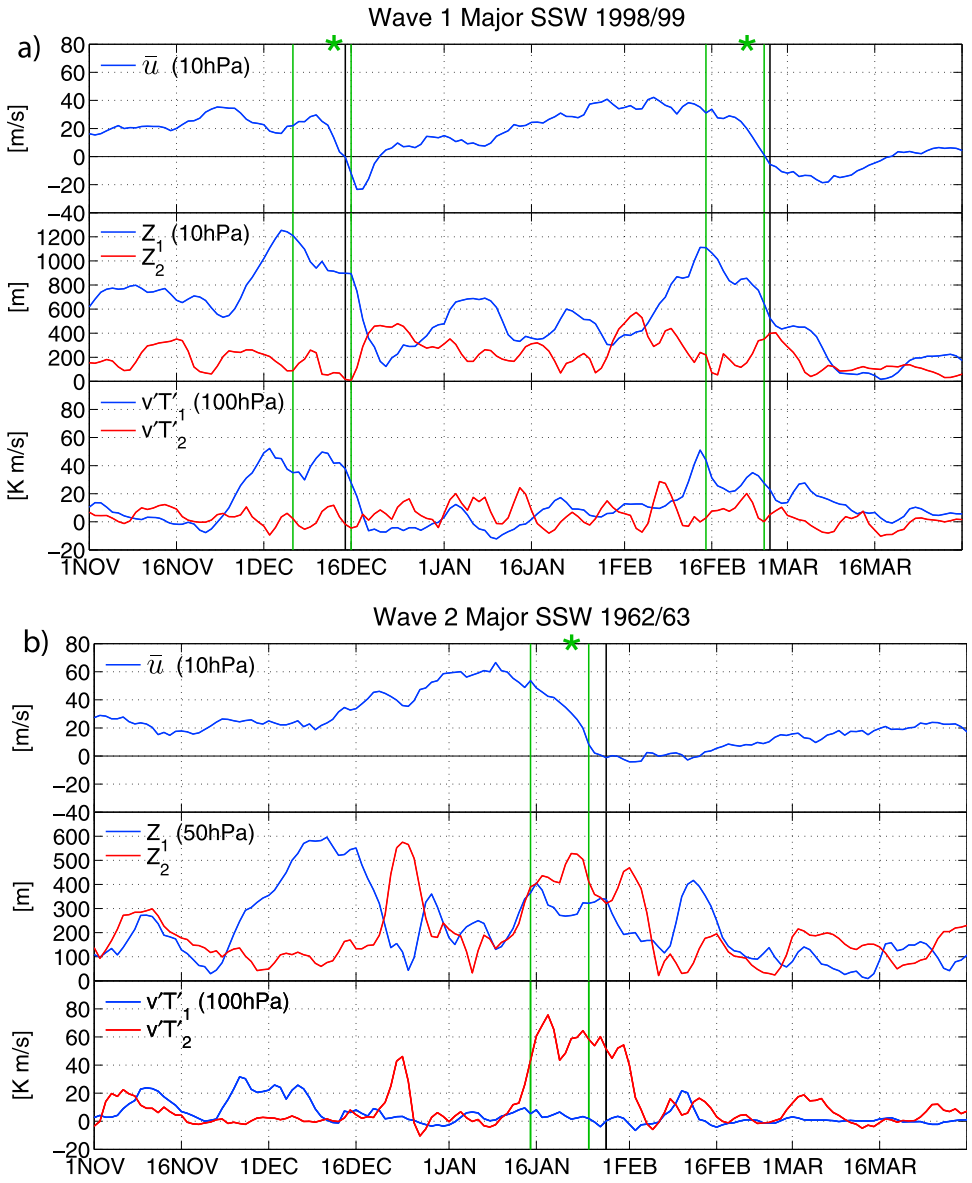

Figure 1. Time series of the ERA-40 zonal mean zonal wind $\bar{u}$ (m/s), the amplitude (m) and the heat flux (K m/s) of $Z_{1,2}$ at 60°N for the indicated pressure levels, from 1 November to 31 March for (a) wavenumber-1 NH winter 1998/99 and (b) wavenumber-2 NH winter 1962/63. The vertical black line indicates the central date of the warming, while the green lines delimit the 10-day window period around the day D (star), in which the identification criterion is applied.

If only the first condition is met, the warming event is classified as W_1 major SSW. If instead the second condition is satisfied at least for 1 day, the warming is classified as W_2 major SSW. The third condition is introduced in order to determine whether the zonal wavenumber-3 may lead to the development of a major SSW. For W_1 major SSWs, the 10 hPa level is chosen because the observed climatological maximum Z_1 is located in the middle to upper stratosphere; whereas for W_2 major SSWs, the 50 hPa level is taken as Z_2 maximizes in the lower to middle stratosphere (not shown here) [*Scaife et al.*, 2000]. The heat flux is analyzed at 100 hPa representative for the planetary wave activity entering the lowermost stratosphere [*Pawson and Kubitz*, 1996; *Newman et al.*, 2001]. The threshold values for W_2 major SSWs of 100 m and 15 K m/s arise from the maximum daily anomalies calculated from the climatology and the major warming composites (not shown here and Figure 3). Even by increasing the threshold values up to 20 percent, does not change the total number of detected W_1 and W_2 major SSWs.

[13] Case studies of W_1 and W_2 major warmings are given in Figure 1, showing time series of $\bar{u}$ at 10 hPa, of $Z_{1,2}$ at 10 or 50 hPa, and of $v'T'_{1,2}$ at 100 hPa (all at 60°N) for the winters 1998/99 and 1962/63. Owing to the large-amplitude increase of Z_1/Z_2 and of the relative heat flux components of $v'T'_1/v'T'_2$ in the 2 to 3 weeks preceding the warming onset, the two major SSWs of the winter 1998/99 are classified as W_1 warmings while the major warming of 28 January 1963

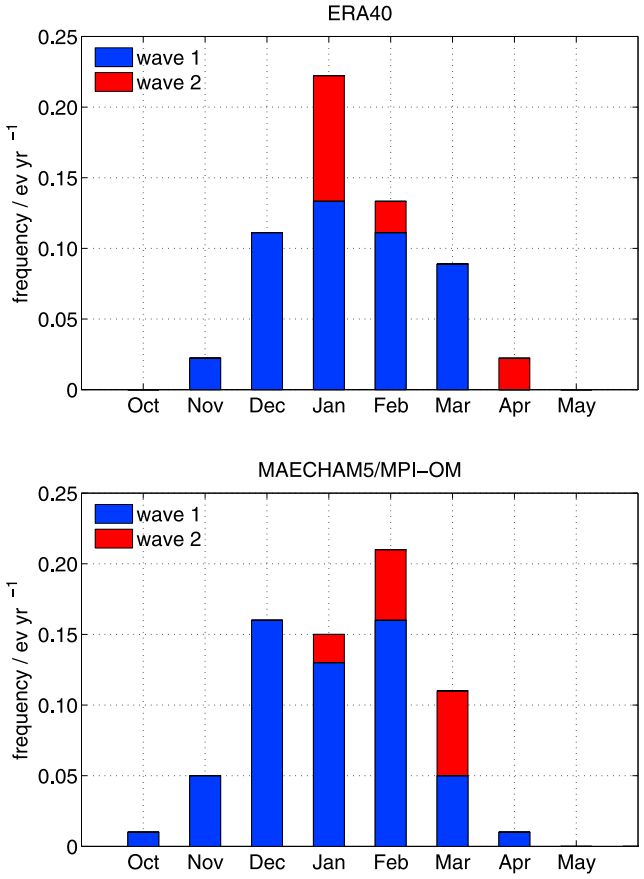

Figure 2. Distribution of major SSWs for ERA-40 and MAECHAM5/MPI-OM data. The blue part of the bars denotes the fraction of zonal W_1 warmings while the red part indicates the zonal W_2 warmings.

is classified as a W_2 event (see also Table 1). The different wave characteristic of these major SSWs was also reported by *Finger and Teweles* [1964], *Manney et al.* [1999], and *Naujokat et al.* [2002].

2.3. Blocking Index

[14] To identify the occurrence of NH circulation blocking events in the middle and high latitudes, we used the blocking index of *Tibaldi and Molteni* [1990], which is based on the criteria proposed by *Lejenäs and Økland* [1983] and *Rex* [1950]. For each longitude of the data grid, the 500 hPa geopotential height gradients *GHGS* and *GHGN* (referring to middle and high latitudes, respectively) are computed daily:

$$GHGS = \frac{Z(\phi_o) - Z(\phi_s)}{(\phi_o - \phi_s)}, \qquad GHGN = \frac{Z(\phi_n) - Z(\phi_o)}{(\phi_n - \phi_o)},$$

where ϕ_n = 80°N + Δ, ϕ_o = 60°N + Δ, ϕ_s = 40°N + Δ, and Δ = −2.5°, 0°, 2.5° both for ERA-40 and MAECHAM5/MPI-OM data. A longitude is then defined as being blocked on a specific day when the following conditions are satisfied for at least one value of Δ:

1) $GHGS > 0$,
2) $GHGN < -10$ m/deg lat.

The blocking indices therefore indicate whether the zonal flow of a given longitude is blocked or not. To represent the intensity of blocking events the gradient *GHGS*, which is essentially proportional to the strength of the geostrophic easterlies, is used. Further space and time constraints are imposed to consider blocking events of sufficient duration; the local blocklike flow pattern must exists over three or more adjacent longitudes and last for 5 or more days. To locate the longitude of the strongest blocking, the maximum *GHGS* is applied, calculated for geopotential height differences between northern and southern midlatitudes.

3. Results

[15] In this section the analyses of major SSWs and tropospheric blocking events are presented. The major SSW climatologies obtained with our criterion for ERA-40 and MAECHAM5/MPI-OM data are shown first. W_1 and W_2 major warming composites are calculated for the wave amplitudes and the heat fluxes. The frequency distribution of tropospheric blocking events is then analyzed. Finally, the connection between major SSWs and blocking events is examined using composites of blocking activity prior to and after the warmings onset.

3.1. Major SSWs Analysis

[16] Figure 2 shows the seasonal distributions of major SSWs for ERA-40 and MAECHAM5/MPI-OM data. Canadian warmings, which can be occasionally associated with the reversal of $\bar{u}$ [*Labitzke*, 1977], are included in the distributions if they fulfill the criterion described above (section 2.2). The relative frequency of major SSWs is obtained by dividing the total number of events per month by the total number of observed years. The whole bar in Figure 2 is relative to all counted events during 1 month while the blue and the red parts represent the fraction (percentage) of W_1 and W_2 major warmings.

[17] In the reanalysis, major warmings occur between November and April with most events happening during January, when the maximum occurrence frequency of 0.22 is found. On average the number of major SSWs per year is 0.6 which corresponds to six events per decade. Of the events occurring in February–March, half are due to a second major SSW (not shown), suggesting a 50 percent chance of a second warming event to occur in late boreal winter.

[18] In the MAECHAM5/MPI-OM model, major SSWs are detected between October and April with most events simulated in December, January, and February. The highest monthly occurrence frequency is found during February (value of 0.21), while 0.7 events per year or seven events per decade are detected on average. Also, in 9 years of the model simulation, second major warming events are detected during February, March, and April (not shown).

[19] The comparison of the two distributions shows that the major warming occurrence is higher in the model. This may be a consequence of the ENSO phenomenon, whose frequency is higher in MAECHAM5/MPI-OM (period of 4 years) than in the reanalysis (period of 4–6 years) [*Jungclaus et al.*, 2006]. The development of major SSWs is in fact facilitated by warm ENSO events, during which enhanced planetary wave disturbances lead to a general weakening of the polar vortex [*Manzini et al.*, 2006]. However, the frequency of observed major warmings can be higher as well. An increase of events was in fact observed

Table 2. Summary Statistics for ERA-40 and MAECHAM5/MPI-OM Data[a]

Data	Total mSSWs	W_1 mSSWs	W_2 mSSWs	mSSWs/Winter	Ratio W_2/W_1
ERA-40	27	21	6	0.60	0.29
MAECHAM5/MPI-OM	70	57	13	0.70	0.23

[a]The abbreviation mSSWs stands for major SSWs.

between 1998/99 and 2008/09 when 11 major SSWs were detected within 11 years [*Manney et al.*, 2005, 2008, 2009; *Labitzke et al.*, 2002]. The main difference between the two distributions is the seasonality of major SSWs: while in ERA-40 most events are identified in January, in MAECHAM5/MPI-OM they occur in February. This tendency of more late winter major SSWs is due to the wintertime extratropical stratospheric circulation of the model, which is characterized by different strength and location of the polar night jet compared to the reanalysis. Another notable difference of MAECHAM5/MPI-OM is the occurrence of one event at the end of October and the larger number of December major warmings. In contrast to previous MAECHAM5 simulations [*Charlton et al.*, 2007], this illustrates an improvement of the seasonal distribution of major SSWs in MAECHAM5/MPI-OM, especially by removing the high bias of early major warming during November and by increasing the number of midwinter events.

[20] From the major SSW distribution, the different amount of W_1 and W_2 warmings is also noticeable. Of the 27 major SSWs detected in ERA-40, 21 are identified as W_1 major warmings while only 6 are W_2 events (Table 1). This gives a W_2/W_1 major SSW ratio of 0.29. Figure 2 shows, for ERA-40 data, that most W_2 events take place in January (frequency of 0.09), but some events occur also in February and April. The January cases are those of 1963, 1968, 1971, and 1985, the February event is that of 1979, while the April W_2 major warming occurred in 1965 (Table 1). Note that our objective algorithm identifies therefore more W_2 cases compared to the so far reported W_2 major SSWs of January 1963, January 1985, and February 1989 [*Naujokat and Labitzke*, 1993; *Krüger et al.*, 2005], which were identified based on a subjective inspection. The event of February 1989 was classified as a final major warming [*Labitzke et al.*, 2002], which is not counted as a major SSW in our algorithm as well.

[21] In MAECHAM5/MPI-OM data, a total of 70 major SSWs is detected. The number of W_1 and W_2 events is 57 and 13, respectively, with a W_2/W_1 major SSW ratio of 0.23. The seasonal distribution demonstrates that for MAECHAM5/MPI-OM, the W_2 events occur in January, February, and March, with the latter having the highest occurrence frequency (value of 0.06). Interestingly, more than half of the major SSWs occurring in March are W_2 events. The similar W_2/W_1 major SSW ratios of the two data sets highlight the ability of the model to simulate W_2 major warmings, although the maximum frequencies occur later. Note that no wavenumber-3 major warming was found in either data set, although three major SSWs characterized by an additionally enhanced wave amplitude of Z_3 were detected in MAECHAM5/MPI-OM (not shown). Table 2 summarizes briefly our results.

[22] The comparison of the ERA-40 major SSWs climatology with the one of *Charlton and Polvani* [2007] reveals that our algorithm leads to a small reduction of the observed number of detected events. While *Charlton and Polvani* [2007] identified 29 events, our algorithm finds only 27 major warmings. This is due to the fact that with our criterion fewer late winter major SSWs are detected: the events of February 1984, March 1988, and February 1989, classified as major SSWs by *Charlton and Polvani* [2007], are in fact identified as final major warmings, which is in good agreement with the long time monitoring by *Labitzke et al.* [2002]. As we detect one major warming in April 1965 (Table 1), we determine in total two events less compared to *Charlton and Polvani* [2007].

[23] *Charlton and Polvani* [2007] investigated the postwarming phase of major SSWs, distinguishing between vortex displacement and vortex splitting events according to whether the major warming leads to a shift of the polar vortex off the pole or to a breakup into two pieces. From this analysis the authors derived a vortex splitting/vortex displacement ratio of 0.93, which is significantly different from our W_2/W_1 major SSWs preconditioning ratio of 0.29. Comparing the same detected major warming events of our Table 1 with Table 1 of *Charlton and Polvani* [2007], we find that all identified W_2 major SSWs during the preconditioning lead to vortex split events in the postphase of major warmings and that all reported displacement events are preceded by W_1 major SSWs. However, there are 7 from the 21 W_1 major SSW cases that lead to split events. This allows us conclude that W_1 major SSWs do not necessarily result in vortex displacement events. Subcomposites for W_1 major SSWs reveal that the seven "W_1-splitting events" are characterized by an enhanced positive anomaly of $v'T'_2$ during the 10 days preceding the warming, in contrast to the 14 "W_1-displacement events" characterized by a weaker anomaly of $v'T'_2$ and a more persistent anomaly of $v'T'_1$ within the 20 days preceding the major warming (not shown here).

[24] The different planetary wave behavior for the two warming types is highlighted in Figure 3 which shows, for W_1 and W_2 major SSWs, composites of daily anomalies of the amplitude of $Z_{1,2}$ at 50 hPa and of the heat fluxes $v'T'_{1,2}$ at 100 hPa, both at 60°N for the period −30 to +30 days of the central date. The statistical significance of the composites is obtained with a t-test, comparing the years with W_1/W_2 major warmings with the years without any. The t-test shows when the anomalies are significantly different from zero at the 95% level.

[25] W_1 major warmings are preceded by an anomalous amplitude increase of Z_1 within 20 days before the central date with an amplitude anomaly of more than 100 m close to the warmings onset in both data sets. In the postwarming phase the anomaly reduces until significant negative anomalies occur between day +15 and +30. In contrast, Z_2 has for most of the time interval negative anomalies, which becomes partly significant in the postwarming phase.

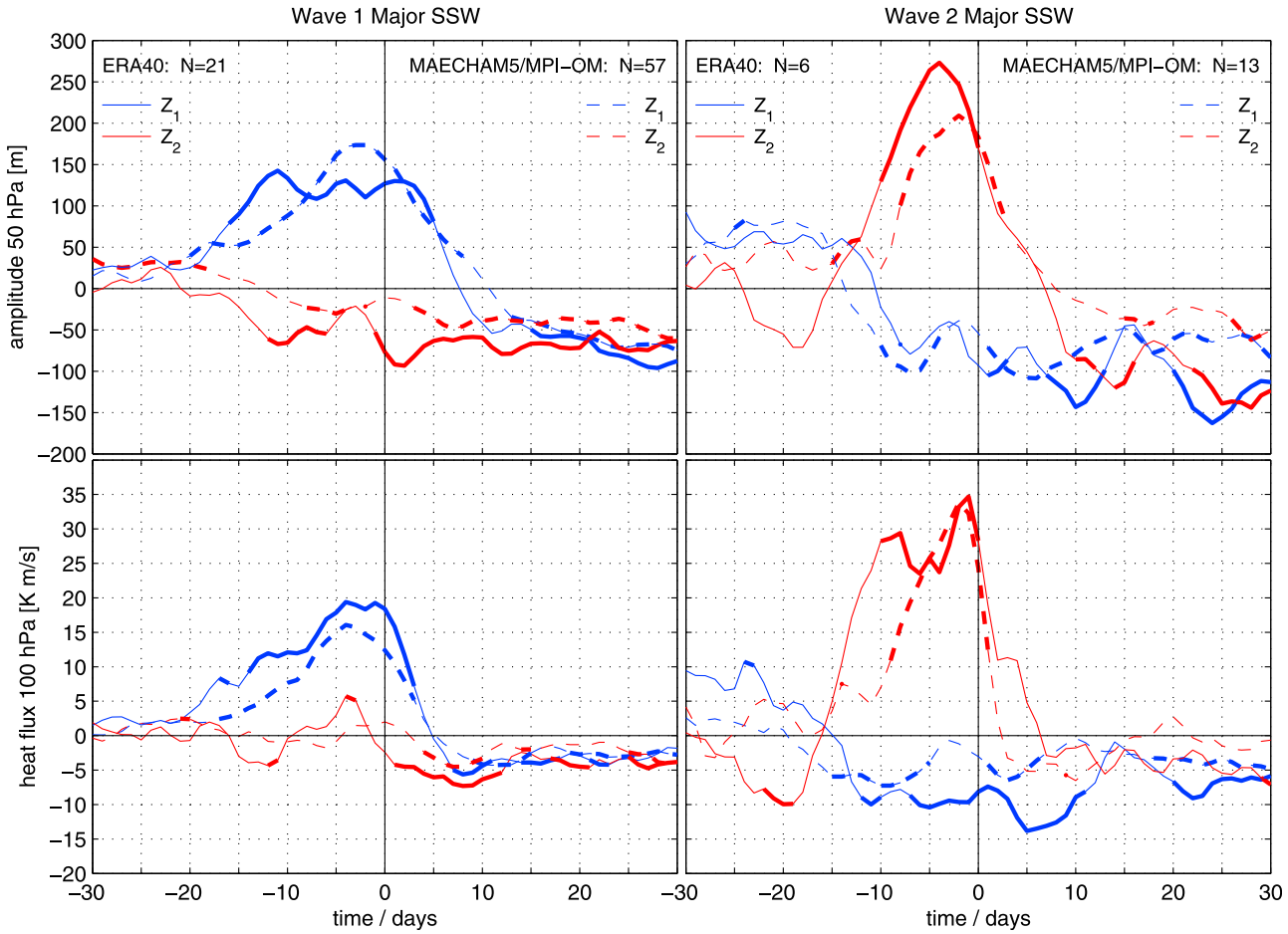

Figure 3. Composites of daily anomalies of the amplitude (m) at 50 hPa and the heat flux (K m/s) at 100 hPa of $Z_{1,2}$ through 60°N for (left) W_1 and (right) W_2 major SSWs of ERA-40 (solid lines) and MAECHAM5/MPI-OM data (dashed lines). N indicates the number of events used for the composites, while day zero refers to the central date of the warmings. Thick line segments indicate anomalies significantly different from zero at the 95% confidence level (t-test).

The heat flux composites highlight the development of W_1 major SSWs. The positive anomaly of $v'T'_1$ in the 3 weeks preceding the warmings onset denotes indeed the major role of W_1 activity entering the lower stratosphere. The anomaly maxima of 19 and 16 K m/s for ERA-40 and MAECHAM5/MPI-OM, respectively, are reached within 5 days prior to the central date. Following the major SSWs there are significant negative heat flux anomalies, indicating suppressed vertical fluxes of Z_1 and Z_2. During the whole 60 days the role of zonal wavenumber-2 is negligible.

[26] The W_2 major warming composites present different characteristics: the main feature is the significant positive amplitude anomaly of Z_2 during the 10 days preceding the central date (values above 150 m larger than normal). An anomalous amplitude increase of Z_1 is already found in the period 30 to 10 days before the warmings onset, although not significant. Following the major warmings, a significant weakening for both zonal wavenumbers is found. The overall development is similar to the finding of *Labitzke* [1981] who pointed out that an amplification of Z_1 is needed to force a preceding vortex deceleration. This permits Z_2 to grow and to propagate more effectively into the vortex, causing a further deceleration until the breakdown of the vortex is achieved. The involvement of Z_1 in W_2 events was also noted by *Dunkerton et al.* [1981] who found for a simulated W_2 major warming that a preconditioning of the mean flow by the Z_1 activity is likely to be required for the following development of Z_2. Of the six detected W_2 major warmings for ERA-40, four of them have this type of preconditioning (April 1965, January 1968, January 1971, and February 1979, Table 1), while those of January 1963 (Figure 1) and January 1985 are characterized only by the amplification of Z_2 (not shown here). Our results therefore confirm that Z_1 can play a role in the preconditioning of W_2 major SSWs, as 2/3 of the observed events have demonstrated. The overall comparison between ERA-40 and MAECHAM5/MPI-OM composites shows that the reanalysis have stronger Z_2 anomalies, which is a consequence of the smaller sampling size of observed versus simulated W_2 major SSWs (6 versus 13 cases). Furthermore, in contrast to W_1 major warmings, the wave activity after the W_2 warmings onset weakens more quickly. The heat flux composites for W_2 major warmings are characterized by a double and single peak of $v'T'_2$ for ERA-40 and MAECHAM5/

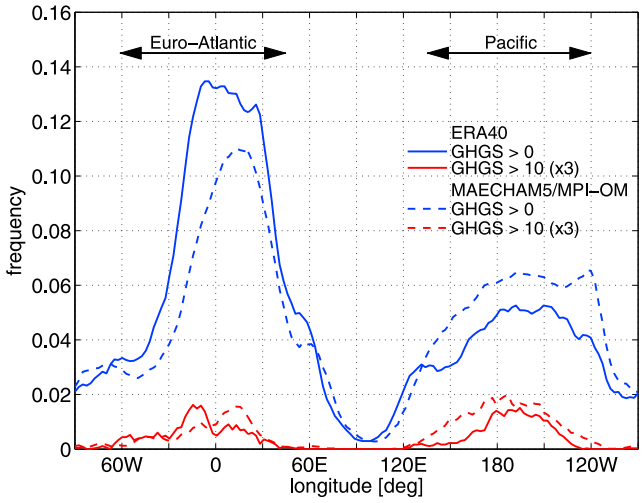

Figure 4. Frequency of ONDJFMAM blocked days as function of longitude for ERA-40 (solid lines) and MAECHAM5/MPI-OM data (dashed lines). Blue lines show the percentage of days characterized by a blocked zonal flow, and red lines are indicative of the percentage of days characterized by a strongly blocked zonal flow. The arrows indicate the Euro-Atlantic (60°W−45°E) and the Pacific (135°E−120°W) sectors. Note that the values of strongly blocked zonal flow (red lines) are multiplied by a factor of three for a better graphical display.

MPI-OM, respectively, which starts 15 and 10 days prior to the central date. The anomaly maxima are almost identical: 35 and 34 K m/s for the reanalysis and the model, respectively. Note that only for the ERA-40 composite a significant positive anomaly of $v'T'_1$ (values up to 11 K m/s) precedes 23 days the large anomaly of $v'T'_2$. As for W_1 major warmings, the heat fluxes display negative anomalies in the postwarming phase. The W_1 seems to only play a role in the −30 to −15 days preceding the central date, from −15 days onward a significant weakening of W_1 (negative anomalies) is evident.

[27] These W_1 and W_2 major warming composites highlight the role of planetary wave activity in preconditioning major SSWs. W_1 major warmings develop with an enhancement of Z_1 only, while W_2 major warmings are generally preceded either by the amplification of Z_2 or by both Z_1 and Z_2 albeit at different time intervals. This characteristic wave evolution of the two types of major warming is in qualitative good agreement with the typical wave activity determined by *Charlton and Polvani* [2007], *Martius et al.* [2009], and *Castanheira and Barriopedro* [2010], who analyzed vortex splitting and displacement events. Their results show in fact that displacement events are preceded by an anomalous increased activity of Z_1, while splitting events require also an amplification of Z_2.

3.2. Tropospheric Blocking Analysis

[28] The overall distribution of blocking events is shown in Figure 4, where the frequency of *blocked days* (i.e., days with a blocked zonal flow) is displayed for each longitude for the October to May period. To demonstrate changes in the blocking intensity, the distribution is illustrated for days characterized by blocked (blue lines) and by strongly blocked zonal flow (red lines), with the latter referring to strong blocking events defined by the spatial and temporal constraints and *GHGS* greater than 10 m/deg lat. If one longitude has a frequency value of 0.1, it means that between October and May (243 days) 24.3 days with a blocked zonal flow occurred within that longitude.

[29] For ERA-40 data, two frequency maxima of 0.13 and 0.05 are detected in the Euro-Atlantic (60°W−45°E) and in the Pacific (135°E−120°W) region, respectively. In MAECHAM5/MPI-OM data, the maxima are shifted eastward by about 30° and have different strengths, with the Euro-Atlantic maximum being weaker than in the reanalysis (frequency of 0.11) and the Pacific one being stronger (values of 0.06). Overall these blocking occurrences are in good agreement with previous studies [*Tibaldi and Molteni*, 1990; *Taguchi*, 2008]. However, *Schalge et al.* [2011] reported that the Tibaldi and Molteni blocking index may be altered by the detection of cutoff lows.

[30] The distributions of strongly blocked days (red lines) have different characteristics between the two data sets. While in ERA-40 the more pronounced peak is found in the Euro-Atlantic region, in MAECHAM5/MPI-OM it is detected in the Pacific region. The model reproduces in fact the number of days with strongly blocked zonal flow in the Euro-Atlantic region (although shifted eastward by about 30°), while it overestimates them in the Pacific region. This may be related to the fact that the model simulates higher 500 hPa geopotential height values over the North Pacific area. Inspecting the standard deviation of the 500 hPa geopotential height fields (not shown) reveals that the model simulates the winter variability in the North Pacific well but not in the North Atlantic, probably resulting in less tropospheric blocking events in the Euro-Atlantic region.

[31] The higher frequency of strong blocking events in the Pacific region can also be seen in Figure 5, where the seasonal distribution of strongly blocked days is shown. The whole bar represents the sum of strongly blocked days in the Euro-Atlantic (blue) and the Pacific sector (red). In both data sets most strong blocking events occur during winter, however, while in ERA-40 the highest number of strongly blocked days is detected in January (value of 2.53) mainly caused by the peak in Euro-Atlantic events, in MAECHAM5/MPI-OM the distribution peaks in February (value of 2.81) mostly because of the high Pacific blocking activity. The model distribution reveals therefore a shift toward late winter. This temporal shift of strong tropospheric blocking events is also reflected by the different seasonal evolution of the 500 hPa geopotential height fields at midlatitudes: while in ERA-40 the highest variability occurs in January, in MAECHAM5/MPI-OM it is found in February (not shown). Noteworthy are also the increased number of simulated strongly blocked days in October, November, March, and May, compared to the reanalysis. ERA-40 shows more days with a strongly blocked zonal flow in the Euro-Atlantic region, whereas MAECHAM5/MPI-OM simulates more in the Pacific region. Overall the seasonal evolution of strong tropospheric blocking events is similar to those of the major SSWs (Figure 2) for which the highest frequencies are found in January and February for the reanalysis and the model respectively.

[32] In the following, the role of tropospheric blocking events preceding major SSWs is analyzed. Figure 6 shows

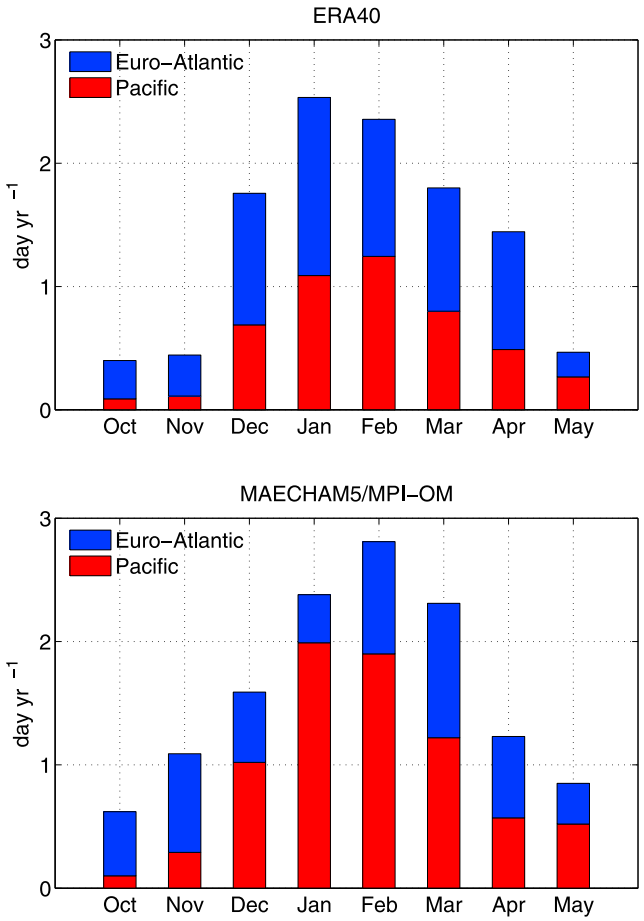

Figure 5. Distribution of strongly blocked days for ERA-40 and MAECHAM5/MPI-OM data. The blue part of the bars denotes the blocked days relative to the Euro-Atlantic sector, while the red part indicates those of the Pacific sector.

W_1 and W_2 major SSWs composites for the daily maximum of *GHGS* in the Euro-Atlantic and the Pacific regions. The statistical significance of the composites is obtained by comparing the time series of the maximum GHGS of single major SSWs with respect to the climatological state, which refers to years without any major SSW. This climatological state is obtained by choosing randomly years without major SSWs.

[33] For ERA-40 W_1 major warmings, a significant increase of the maximum of *GHGS* (values up to 4.0 m/deg lat) is found for the Euro-Atlantic region in the prewarming phase, while a rapid decrease occurs in the following week after warming onset. For the Pacific region, the maximum *GHGS* is weak before the central date but maximizes 5 days after the warmings onset (2.4 m/deg lat), when the minimum in the Euro-Atlantic region is detected. A similar behavior is found for MAECHAM5/MPI-OM, although the prewarming peak in the Euro-Atlantic region is weaker (value of 2.4 m/deg lat) and the postwarming peak in the Pacific region is higher (value of 3.6 m/deg lat), postponed and prolonged by a couple of days. This pronounced Pacific peak arises probably from the stronger and more frequent blocking activity simulated by the model in the Pacific region as shown before in Figures 4 and 5. Thus the model simulates a significant connection between Euro-Atlantic blocking events preceding and Pacific blocking events following W_1 major warmings.

[34] Given the low number of observed events, the W_2 major warming composites for ERA-40 should be interpreted cautiously. Therefore we only want to point out the relatively high maximum *GHGS* for both Euro-Atlantic and Pacific regions prior to the W_2 warmings onset, followed by highest blocking intensity over the Pacific sector in the postwarming phase. Again the high maximum *GHGS* values in these composites are due to the few observed events considered. With the MAECHAM5/MPI-OM model we are now able to analyze the W_2 major warming–blocking relation into more detail given the fact that (1) the model is able to simulate the physical mechanism of W_2 major warmings and (2) we have 13 simulated events to be considered.

[35] For the simulated W_2 major SSWs significant maximum *GHGS* values are analyzed for both regions in the 20 days preceding the central date but with stronger blocking activity in the Pacific sector (values above 4.0 m/deg lat). For both regions, maximum blocking intensity begins to weaken already a couple of days before the central date until it increases again in the postwarming phase around day 5. In the following, postwarming days alternating stronger blocking activities are found in the Pacific and in the Euro-Atlantic sectors.

[36] From ERA-40 and the model analyses we can conclude that W_1 major SSWs can be preceded by blocking activity in the Euro-Atlantic region within 15 days prior to the warming onset. The postwarming phase shows instead a reduction of the blocking activity in the Euro-Atlantic region accompanied by an increase of the activity in the Pacific region. This evolution of the Euro-Atlantic blocking activity is similar to that obtained by *Woollings et al.* [2010], who noted a strengthening of European blocking events prior to major SSWs of displacement type, followed by a reduction of the European blocking activity after the warming event. It is also consistent with the studies of *Martius et al.* [2009] and *Castanheira and Barriopedro* [2010] who pointed out that vortex displacement events are mainly preceded by Euro-Atlantic blocking events.

[37] The W_2 major SSWs composites for MAECHAM5/MPI-OM reveals that in the prewarming phase the strong blocking activity in the Pacific sector can be accompanied by activity in the Euro-Atlantic region. This model finding may be biased by the higher than observed Pacific blocking activity simulated by MAECHAM5/MPI-OM. However, *Martius et al.* [2009] and *Castanheira and Barriopedro* [2010] also found a significant increase of Pacific blocking activity in the prewarming phase of major SSWs, analyzing vortex splitting events. The increased blocking activity of the postwarming phase in both regions was instead underlined by *Woollings et al.* [2010] investigating vortex splitting events as well.

[38] Our analysis of the blocking activity prior to W_1/W_2 major SSWs is therefore in good agreement with the vortex displacement/split studies by *Martius et al.* [2009], *Castanheira and Barriopedro* [2010], and *Woollings et al.* [2010]. In contrast to *Taguchi* [2008] we find significant connections of tropospheric blocking events preceding major SSWs by analyzing different types of major warmings specifying the planetary wave evolvement in the development phase.

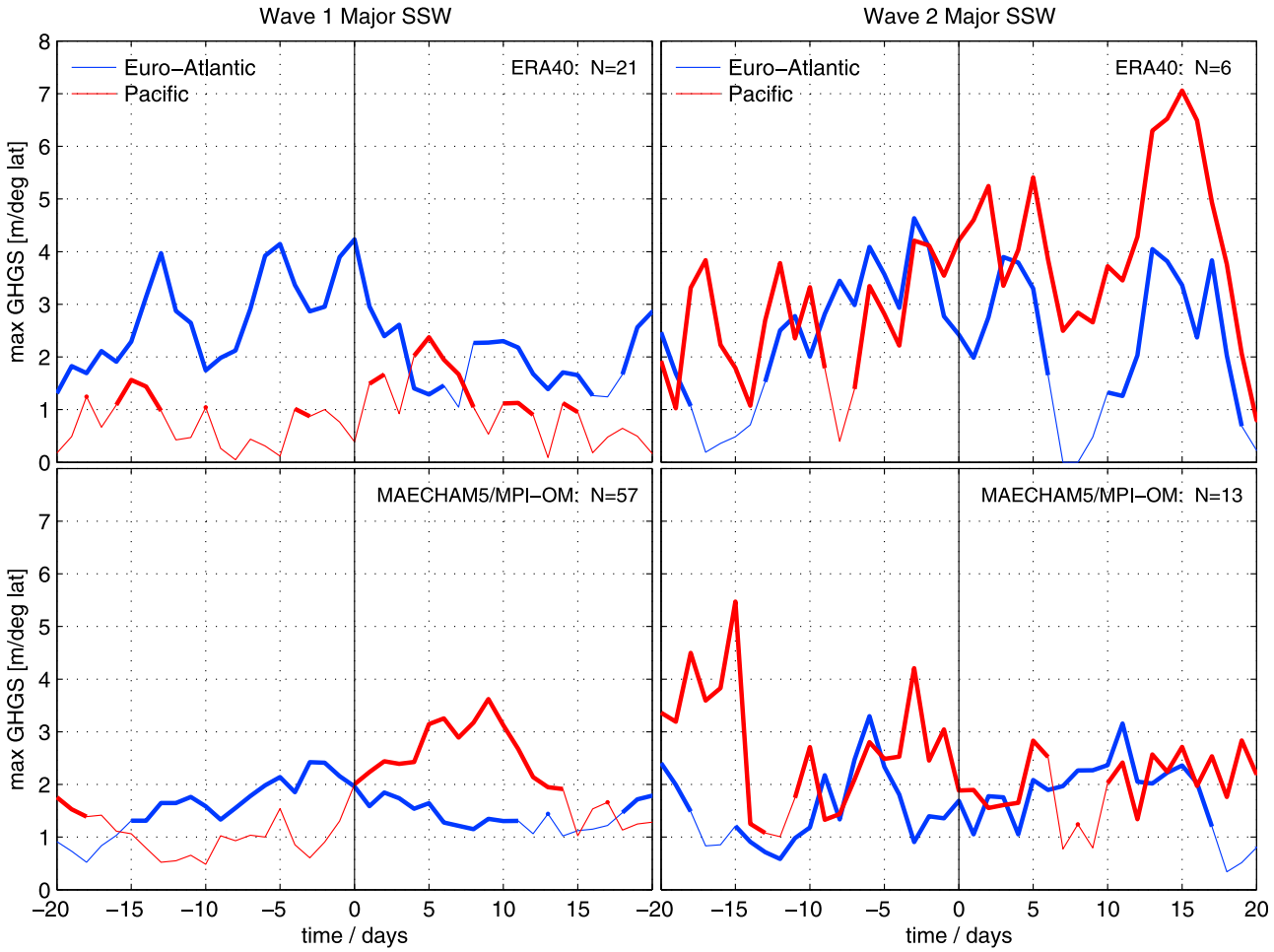

Figure 6. Composites of the daily maximum of the 500 hPa *GHGS* (for $\Delta = -2.5°$) in the Euro-Atlantic (blue line) and Pacific sectors (red line) for (left) W_1 and (right) W_2 major SSWs of (top) ERA-40 and (bottom) MAECHAM5/MPI-OM data. *N* indicates the number of events used for the composites, while day zero refers to the central date of the warmings. Thick line segments indicate that the values are significant at the 95% confidence level (t-test).

However, we would like to stress that as shown by *Taguchi* [2008], not all major SSWs are necessarily preceded by tropospheric blocking activity.

4. Conclusion

[39] In this study the winter variability of the NH stratospheric polar vortex in ERA-40 and MAECHAM5/MPI-OM data is analyzed in detail. An objective algorithm for the identification and classification of major SSWs, considering the development phase, is developed. All detected events are used to compute a major SSW climatology. Different frequencies of major warmings are found for the two data sets: while for ERA-40 the number of events per year is 0.6, for MAECHAM5/MPI-OM it is 0.7. The model tends therefore to simulate a higher number of major SSWs, which is in good agreement with the observed increase of major SSW frequency since the late 1990s. The seasonal distribution of the major warmings reveal occurrences between November and April in the reanalysis and between October and April in the model. The main difference between the two distributions is the shift of the warming occurrence peak: while in ERA-40 most events are identified in January, in MAECHAM5/MPI-OM they occur in February. The coupled middle atmosphere model better simulates the major SSW frequency compared to the previous MAECHAM5 version in which the model does not have an interactive ocean. The number of major warmings in MAECHAM5/MPI-OM is in fact strongly reduced in November and increased in midwinter, thus leading to an improved frequency distribution closer to the reanalysis. The detected major SSWs are distinguished between W_1 and W_2 events, according to the planetary wave activity during the prewarming phase. For the two data sets a similar W_2/W_1 major SSW ratio is found: 0.29 for ERA-40 and 0.23 for MAECHAM5/MPI-OM. The seasonal distribution of W_2 major warmings reveal that most events occur in January for the reanalysis and in March for the model. The different planetary wave behavior for W_1 and W_2 major warmings is confirmed by significant differences in the composite analyses for both data sets. While W_1 events are preceded by an intense activity of Z_1, W_2 major SSWs are preceded either by an intense activity of Z_2 alone or by an intense activity of Z_1, which is followed by a strong intensification

of Z_2. These results highlight the ability of the model to simulate the different W_1 and W_2 major SSWs.

[40] The role of tropospheric blocking events influencing the development of major SSWs is examined in a second step. As expected, the observed frequency climatology of blocking events reveals the maximum for the Euro-Atlantic region and a secondary maximum for the Pacific region. In contrast to ERA-40, the model underestimates the frequency of Euro-Atlantic blocking events and overestimates the frequency of Pacific blocking events. Analyzing strong blocking events, ERA-40 shows an almost equal frequency ratio between strong Euro-Atlantic and strong Pacific events, while a dominance of strong Pacific events is found in MAECHAM5/MPI-OM. The seasonal distribution of tropospheric blocking events displays that most strong events are detected in January for the reanalysis and in February for the model. Examining the W_1/W_2 major SSW composites reveal a significant connection to tropospheric blocking events occurring in the prewarming phase. For W_1 major SSWs we find for both reanalysis and model, that these events are mainly preceded by Euro-Atlantic blocking events. W_2 major warmings are instead mainly preceded by Pacific blocking events in the model, although a weaker blocking activity is also found in the Euro-Atlantic region within 10 days prior to the warmings onset. Overall the major SSW composites show that Euro-Atlantic and Pacific blocking events can be responsible for the amplification of Z_1 and Z_2, respectively, developing into W_1 and W_2 major warmings in good agreement with previous studies.

[41] On the basis of the favorable comparison of our major SSW analysis with previous observational studies, we believe that our algorithm can be a very good model diagnostic for analyzing the physical processes responsible for the development of major warmings. It can be used to investigate the preconditioning of major SSWs in coupled chemistry-climate models and in the new generation of high-top CMIP models. This enables us to better quantify the ability of the models to simulate major SSWs and hence the stratospheric winter variability in past and future climate simulations.

[42] **Acknowledgments.** We are grateful to ECMWF for providing the ERA-40 Reanalysis data. We thank the German Climate Computation Center (DKRZ) Hamburg for providing computing time and Monika Esch from the MPI for running the model experiment. We also gratefully acknowledge the useful comments and suggestions of Douglas Maraun, the anonymous reviewers, the associate editor and the JGR Editor Steven Ghan. The work of this study is funded by the national BMBF joint research project MiKlip within the project ALARM through the grant 01LP1130B.

References

Andrews, D. G., J. R. Holton, and C. B. Leovy (1987), *Middle Atmosphere Dynamics*, 489 pp., Academic, San Diego, Calif.

Butchart, N., et al. (2010), Stratospheric dynamics, in *SPARC CCMVal Report on the Evaluation of Chemistry-Climate Models, WMO/TD–1526*, pp. 109–148, SPARC, World Meteorol. Org., Zurich, Switzerland.

Butchart, N., et al. (2011), Multimodel climate and variability of the stratosphere, *J. Geophys. Res.*, *116*, D05102, doi:10.1029/2010JD014995.

Castanheira, J. M., and D. Barriopedro (2010), Dynamical connection between tropospheric blockings and stratospheric polar vortex, *Geophys. Res. Lett.*, *37*, L13809, doi:10.1029/2010GL043819.

Charlton, A. J., and L. M. Polvani (2007), A new look at stratospheric sudden warmings. Part I: Climatology and modeling benchmarks, *J. Clim.*, *20*, 449–469.

Charlton, A. J., et al. (2007), A new look at stratospheric sudden warmings. Part II: Evaluation of numerical model simulations, *J. Clim.*, *20*, 470–488.

Dunkerton, T., C. P. Hsu, and M. E. McIntyre (1981), Some eulerian and Lagrangian diagnostics for a model stratospheric warming, *J. Atmos. Sci.*, *38*, 819–843.

Finger, F. G., and S. Teweles (1964), The mid-winter 1963 stratospheric warming and circulation change, *J. Appl. Meteorol.*, *3*, 1–15.

Fortuin, P. J. F., and H. Kelder (1998), An ozone climatology based on ozonesonde and satellite measurements, *J. Geophys. Res.*, *103*(D24), 31,709–31,734.

Garfinkel, C. I., D. L. Hartmann, and F. Sassi (2010), Tropospheric precursors of anomalous Northern Hemisphere stratospheric polar vortices, *J. Clim.*, *23*, 3282–3299.

Giorgetta, M. A., E. Manzini, M. Esch, and E. Roeckner (2007), Role of the stratosphere in climate modelling: The connection between the Hadley and the Brewer-Dobson Circulation, paper presented at Chapman Conference on the Role of the Stratosphere in Climate and Climate Change, AGU, Santorini, Greece.

Hines, C. O. (1997a), Doppler spread parameterization of gravity wave momentum deposition in the middle atmosphere. Part I: Basic formulation, *J. Atmos. Sol. Terr. Phys.*, *59*, 371–386.

Hines, C. O. (1997b), Doppler spread parameterization of gravity wave momentum deposition in the middle atmosphere. Part II: Broad and quasi monochromatic spectra and implementation, *J. Atmos. Sol. Terr. Phys.*, *59*, 387–400.

Jungclaus, J. H., et al. (2006), Ocean circulation and tropical variability in the coupled model ECHAM5/MPI-OM, *J. Clim.*, *19*, 3952–3972.

Krüger, K., B. Naujokat, and K. Labitzke (2005), The unusual midwinter warming in the Southern Hemisphere stratosphere 2002: A comparison to Northern Hemisphere phenomena, *J. Atmos. Sci.*, *62*, 603–613.

Labitzke, K. (1965), On the mutual relation between stratosphere and troposphere during periods of stratospheric warmings in winter, *J. Appl. Meteorol.*, *4*, 91–99.

Labitzke, K. (1977), Interannual variability of the winter stratosphere in the Northern Hemisphere, *Mon. Weather Rev.*, *105*, 762–770.

Labitzke, K. (1981), The amplification of height wave 1 in January 1979: A characteristic precondition for the major warming in February, *Mon. Weather Rev.*, *109*, 983–989.

Labitzke, K., et al. (2002), *The Berlin Stratospheric Data Series* [CD-ROM], Meteorol. Inst., Free Univ. Berlin, Berlin.

Langematz, U., M. Kunze, K. Krüger, K. Labitzke, and G. L. Roff (2003), Thermal and dynamical changes of the stratosphere since 1979 and their link to ozone and CO_2 changes, *J. Geophys. Res.*, *108*(D1), 4027, doi:10.1029/2002JD002069.

Lejenäs, H., and H. Økland (1983), Characteristic of Northern Hemisphere blocking as determined from a long time series of observational data, *Tellus, Ser. A*, *35*, 350–362.

Limpasuvan, V., D. W. J. Thompson, and D. L. Hartmann (2004), The life cycle of the Northern Hemisphere sudden stratospheric warmings, *J. Clim.*, *17*, 2584–2596.

Lott, F. (1999), Alleviation of stationary biases in a GCM through a mountain drag parameterization scheme and a simple representation of mountain lift forces, *Mon. Weather Rev.*, *127*, 788–801.

Lott, F., and M. J. Miller (1997), A new-subgrid-scale orographic drag parameterization: Its formulation and testing, *Q. J. R. Meteorol. Soc.*, *123*, 101–127.

Manney, G. L., W. A. Lahoz, R. Swinbank, A. O'Neill, P. M. Connew, and R. W. Zurek (1999), Simulation of the December 1998 stratospheric major warming, *Geophys. Res. Lett.*, *26*, 2733–2736.

Manney, G. L., K. Krüger, J. L. Sabutis, S. A. Sena, and S. Pawson (2005), The remarkable 2003–2004 winter and other recent warm winters in the Arctic stratosphere since the late 1990s, *J. Geophys. Res.*, *110*, D04107, doi:10.1029/2004JD005367.

Manney, G. L., et al. (2008), The evolution of the stratopause during the 2006 major warming: Satellite data and assimilated meteorological analyses, *J. Geophys. Res.*, *113*, D11115, doi:10.1029/2007JD009097.

Manney, G. L., M. J. Schwartz, K. Krüger, M. L. Santee, S. Pawson, J. N. Lee, W. H. Daffer, R. A. Fuller, and N. J. Livesey (2009), Aura Microwave Limb Sounder Observations of Dynamics and Transport during the record-breaking 2009 Arctic stratospheric Major Warming, *Geophys. Res. Lett.*, *36*, L12815, doi:10.1029/2009GL038586.

Manzini, E., N. A. McFarlane, and C. McLandress (1997), Impact of the Doppler spread parameterization on the simulation of the middle atmosphere circulation using the MA/ECHAM4 general circulation model, *J. Geophys. Res.*, *102*(D22), 25,751–25,762.

Manzini, E., M. A. Giorgetta, M. Esch, L. Kornblueh, and E. Roeckner (2006), The influence of sea surface temperatures on the northern winter stratosphere: Ensemble simulations with the MAECHAM5 model, *J. Clim.*, *19*, 3863–3881.

Martius, O., L. M. Polvani, and H. C. Davies (2009), Blocking precursors to stratospheric sudden warming events, *Geophys. Res. Lett.*, *36*, L14806, doi:10.1029/2009GL038776.

Matsuno, T. (1970), Vertical propagation of stationary planetary waves in the winter Northern Hemisphere, *J. Atmos. Sci.*, *27*, 871–883.

Matsuno, T. (1971), A dynamical model on stratospheric warmings, *J. Atmos. Sci.*, *28*, 1479–1494.

Mukougawa, H., and T. Hirooka (2004), Predictability of stratospheric sudden warming: A case study for 1998/99 winter, *Mon. Weather Rev.*, *132*, 1764–1776.

Naujokat, B., and K. Labitzke (1993), *Collection of Reports on the Stratospheric Circulation During the Winters 1974/75-1991/92: Japanese Solar Terrestrial Energy Program Handbook*, 301 pp., SCOSTEP Bur., Urbana, Ill.

Naujokat, B., and H. K. Roscoe (2005), Evidence against an Antarctic stratospheric vortex split during the periods of pre-IGY temperature measurements, *J. Atmos. Sci.*, *62*, 885–889.

Naujokat, B., K. Krüger, K. Matthes, J. Hoffmann, M. Kunze, and K. Labitzke (2002), The early major warming in December 2001—Exceptional?, *Geophys. Res. Lett.*, *29*(21), 2023, doi:10.1029/2002GL015316.

Newman, P. A., and J. E. Rosenfield (1997), Stratospheric thermal damping times, *Geophys. Res. Lett.*, *24*(4), 433–436.

Newman, P. A., E. R. Nash, and J. E. Rosenfield (2001), What controls the temperature of the Arctic stratosphere during the spring?, *J. Geophys. Res.*, *106*(D17), 999–20,010, doi:10.1029/2000JD000061.

O'Neill, A., and B. F. Taylor (1978), A study of the major stratospheric warming of 1976/77, *Q. J. R. Meteorol. Soc.*, *105*, 71–92.

Pawson, S., and T. Kubitz (1996), Climatology of planetary waves in the northern stratosphere, *J. Geophys. Res.*, *101*(D12), 16,987–16,996.

Pawson, S., et al. (2000), The GCM-reality intercomparison project for SPARC (GRIPS): Scientific issues and initial results, *Bull. Am. Meteorol. Soc.*, *81*, 781–796.

Quiroz, R. (1986), The association of stratospheric warmings with tropospheric blocking, *J. Geophys. Res.*, *91*(D4), 5277–5285.

Reed, R. J. (1963), On the cause of the stratospheric sudden warming phenomenon, *Meteorol. Abhand.*, *36*, 315–334.

Rex, D. R. (1950), Blocking action in the middle troposphere and its effect upon regional climate. II: The climatology of blocking actions, *Tellus*, *2*, 275–302.

Roeckner, E., et al. (2006), Sensitivity of simulated climate to horizontal and vertical resolution in the ECHAM5 atmosphere model, *J. Clim.*, *19*, 3771–3791.

Scaife, A. A., J. Austin, N. Butchart, S. Pawson, M. Keil, J. Nash, and I. N. James (2000), Seasonal and interannual variability of the stratosphere diagnosed from UKMO TOVS analyses, *Q. J. R. Meteorol. Soc.*, *126*, 2585–2604.

Schalge, B., R. Blender, and K. Fraedrich (2011), Blocking detection based on synoptic filters, *Adv. Meteorol.*, *2011*, 717812, doi:10.1155/2011/717812.

Taguchi, M. (2008), Is there a statistical connection between stratospheric sudden warming and tropospheric blocking events?, *J. Atmos. Sci.*, *65*, 1442–1454.

Tibaldi, S., and F. Molteni (1990), On the operational predictability of blocking, *Tellus, Ser. A*, *42*, 343–365.

Uppala, S. M., et al. (2005), The ERA-40 re-analysis, *Q. J. R. Meteorol. Soc.*, *131*, 2961–3012.

Wetzel, P., H. Haak, J. Jungclaus, and E. Maier-Reimer (2010), The Max-Planck-Institute global Ocean/Sea-Ice model MPI-OM, technical report, Max-Planck-Inst. for Meteorol., Hamburg, Germany. [Available at http://www.mpimet.mpg.de/en/wissenschaft/modelle/mpiom.html.]

Woollings, T., A. Charlton-Perez, S. Ineson, A. G. Marshall, and G. Masato (2010), Associations between stratospheric variability and tropospheric blocking, *J. Geophys. Res.*, *115*, D06108, doi:10.1029/2009JD012742.

S. Bancalá and K. Krüger, GEOMAR, Helmholtz Centre for Ocean Research Kiel, Duesternbrooker Weg 20, D-24105 Kiel, Germany. (sbancala@geomar.de; kkrueger@geomar.de)

M. Giorgetta, Max Planck Institute for Meteorology, Bundesstr. 53, D-20146 Hamburg, Germany. (marco.giorgetta@zmaw.de)